PROCESSING *PP* AND *PS* WAVES IN MULTICOMPONENT SEA-FLOOR DATA FOR AZIMUTHAL ANISOTROPY: THEORY AND OVERVIEW

X. Y. LI

Edinburgh Anisotropy Project[1]

TRAITEMENT DES DONNÉES MULTICOMPOSANTES EN ONDES PP ET PS SUR LES FONDS MARINS, EN TERMES D'ANISOTROPIE AZIMUTALE : THÉORIE ET VUE D'ENSEMBLE

Dans l'hypothèse d'une anisotropie azimutale induite par les fractures, nous révisons la théorie et développons des méthodes de traitement pour retrouver l'orientation et la densité de la fracture à partir de données sur les fonds sous-marins à composantes multiples.

Les variations azimutales d'amplitude PP, la vitesse de move-out et le move-out d'intervalle présentent des variations elliptiques dans un milieu azimutalement anisotrope. Ceci peut servir à déterminer l'azimut de la fracture et a été vérifié sur des données réelles. Mais les effets sur les ondes P interviennent seulement sur des azimuts multiples et d'autres facteurs en compliquent l'analyse. Ceci limite dans une certaine mesure l'application de l'analyse des ondes P. L'analyse des ondes PS peut de ce fait s'avérer très utile. Pour des ondes PS dont la propagation est proche de la verticale, la polarisation et la différence de temps de propagation des ondes transversales permettent une mesure directe de l'orientation et de l'intensité de la fracturation. Pour une acquisition en 2D où le profil est parallèle au câble récepteur, une méthode optimale est proposée pour déterminer l'azimut de la fracture à partir de l'azimut de polarisation de l'onde transversale rapide. La méthode utilise l'analyse des rotations et suppose que les ondes transversales rapides et lentes ont des formes d'onde similaires. Pour une géométrie transversale en 3D où le profil est perpendiculaire au câble récepteur, deux méthodes de détermination sont proposées. La première repose sur le changement de polarité et la diminution de l'amplitude dans les regroupements azimutaux de la composante géophonique transversale. La seconde méthode implique une rotation de paires orthogonales de regroupements azimutaux du récepteur-source. L'azimut de polarisation que l'on a déterminé permet ensuite de dissocier les ondes transversales rapides et lentes dans les regroupements de champs directs pour estimer le temps de propagation.

Assuming fracture-induced azimuthal anisotropy, we review the theory and develop processing methods for recovering the fracture orientation and density from multicomponent sea-floor data.

(1) British Geological Survey,
Murchison House,
West Mains Road,
Edinburgh EH9 3LA,
Scotland - United Kingdom

The azimuthal variations in PP amplitude, normal move-out velocity, and interval move-out show elliptical variations in an azimuthally anisotropic medium. This can be used to determine the fracture strike of the medium and has been verified from real data. However, the P-wave effects only occur with multi-azimuths, and are often complicated by other factors. This limits the application of P-wave analysis to some extent. Analysis of PS waves may thus prove to be beneficial. For near vertical propagating PS waves, the polarization and time delay of the shear-waves provide a direct measurement of the fracture orientation and intensity. For a 2D acquisition where the survey line is along the receiver cable, an optimum method is proposed for determining the fracture strike from the polarization azimuth of the fast shear-wave. The method uses rotation analysis and assumes that the fast and slow shear-waves have similar waveforms. For a 3D cross geometry where the survey line is perpendicular to the receiver cable, two deterministic methods are proposed. The first one is based on the polarity change and amplitude dimming in the azimuthal gathers of the transverse-geophone component. The second one involves a rotation of orthogonal pairs of source-receiver azimuthal gathers. The determined polarization azimuth can then be used to separate the fast and slow shear waves in the inline-shooting gathers for time-delay estimation.

TEORÍA RELATIVA A LAS ONDAS PP Y PS POR ANISOTROPÍA AZIMUTAL TOMANDO COMO PUNTO DE PARTIDA LOS DATOS RELATIVOS A LOS FONDOS SUBMARINOS DE COMPONENTES MÚLTIPLES

Situándose en la hipótesis de una anisotropía azimutal inducida de una fractura, el autor ha revisado la teoría y desarrollado métodos de procesamiento para restablecer la orientación y la densidad de la fractura tomando como punto de partida los datos relativos a los fondos submarinos de componentes múltiples.

Las variaciones azimutales de amplitud PP, la velocidad normal de desplazamiento y el desplazamiento intermedio presentan variaciones elípticas en un medio azimutalmente anisótropo. Esto puede servir para determinar el impacto de la fractura del medio y se ha verificado por utilización de datos reales. Pero los efectos de las ondas P únicamente intervienen en el caso de desplazamientos suficientemente amplios de azimuts múltiples y de otros factores que vienen a complicar el análisis. En cierto modo, todo ello limita la aplicación del análisis de las ondas P. Por ello, el análisis de las ondas PS puede resultar sumamente útil a este respecto. Para las ondas PS, cuya propagación es cercana de la vertical, la polarización y el tiempo de propagación de las ondas transversales permiten obtener una medición directa de la orientación y de la intensidad de la fractura. Para una localización en 2D en la cual el trazado es paralelo al cable receptor, se propone un método óptimo para determinar el impacto de la fractura tomando como punto de partida el azimut de polarización de la onda transversal rápida. En este método se aplica el análisis de las rotaciones suponiendo que las ondas transversales rápidas y lentas son de forma similar. Para una geometría transversal en 3D en cuyo caso el trazado es perpendicular al cable receptor, se proponen dos métodos de determinación. El primero se funda en el cambio de polaridad, la disminución de la amplitud en las reagrupaciones azimutales de la componente geofónica transversal. El segundo método presupone una rotación de pares ortogonales de reagrupaciones azimutales del receptor-fuente. El azimut de polarización que se ha determinado permite, acto seguido, disociar las ondas transversales rápidas y lentas en las reagrupaciones de campos directos para evaluar el tiempo de propagación.

INTRODUCTION

With the advent of multicomponent sea-floor seismic technology, the study of mode converted shear-waves has become increasingly common in the industry. The mode converted wave retains the benefit of both *P-* and *S*-wave surveys (Li *et al.,* 1996) and offers the potential for more cost-effective reservoir characterization and monitoring. However, due to the asymmetrical ray path, processing and interpreting mode-converted waves requires more effort than single-mode *P-* and *S*-waves. For anisotropy analysis, there are additional difficulties in determining the polarization of the fast split shear-wave, compared with multicomponent land shear-wave data.

Crampin (1981) gave a fundamental review of wave propagation in anisotropic media, and the effects of anisotropy examined in his paper are mainly illustrated from numerical solutions. Thomsen (1986, 1988) presented these effects within the context of exploration geophysics, and introduced some analytical formulations of these effects under the assumption of weak anisotropy. Recently, Tsvankin (1996) gave a complete review of the effects of *P*-wave propagation in a transversely isotropic medium with a vertical symmetry axis (TIV) and illustrated the effects mainly from approximate analytical solutions.

In this paper, I examine some of the fundamental aspects for both *PP* and *PS* waves propagating in fracture-induced transversely anisotropic media with a horizontal symmetry axis (TIH). I also study the amplitude behaviour and velocity effects for *P*-waves, and the polarization direction and time delay for *PS* waves. All these effects are expressed in analytical forms under the assumption of weak anisotropy, which provides some insights into the various dependencies, and allows the development of processing algorithms to extract these effects from multicomponent seismic data. Although I have formulated these algorithms in the context of sea-floor recording, the concepts can also be applied to other forms of acquisition geometry, such as walkway VSPs, and vertical cable seismics.

The effects of azimuthal anisotropy for *P*-waves are relatively well known. For amplitude effects, there are Lefeuvre (1994), Mallic *et al.* (1996), Lynn *et al.* (1996), Rüger (1996), Li and Mavko (1996), MacBeth *et al.* (1997), and among others. For velocity and move-out effects, there are Sena (1991), Li and Crampin (1993), Tsvankin (1995), Grechka and Tsvankin (1996),

Corrigan *et al.* (1996), Li (1997) and among others. However, the effect of azimuthal anisotropy on *PS* wave amplitudes is not well understood. Li *et al.* (1996) first presented the *PS* AVO equations for anisotropic media, and they conclude that *PS* AVO and its azimuthal variations may be more sensitive to fractures. In contrast, The variations of *PS* wave polarizations and time delays are better understood arising from *SS* studies. For near-vertical propagations, the polarization of the fast shear-wave is parallel to the fracture strike, and the time delay between the two split shear-waves is proportional to the fracture density.

In the following sections, I will present the basic theory, compare the AVO responses of *PP* and *PS* waves and review *P*-wave processing methods for a fractured-induced TIH medium. This is followed by development of *PS* wave processing methods for estimating the fracture strike and density.

1 BASIC THEORY

A medium containing aligned vertical fractures gives rise to transverse isotropy with a horizontal axis of symmetry (TIH). This is the simplest form of azimuthal anisotropy with only five elastic constants, and is the main subject of this paper. In the natural coordinate system, containing the fracture normal and strike, and the vertical axis, the stiffness tensor of this TIH medium can be written as:

$$C = \begin{pmatrix} C_{11} & C_{13} & C_{13} & & & \\ C_{13} & C_{33} & C_{33}-2C_{44} & & 0 & \\ C_{13} & C_{33}-2C_{44} & C_{33} & & & \\ & & & C_{44} & & \\ & 0 & & & C_{66} & \\ & & & & & C_{66} \end{pmatrix} \quad (1)$$

Often a seismic survey line is at an oblique angle to the fracture strike, and the fracture strike and the fracture density need to be determined from the acquired data. The wavefield in the acquired data is governed by a new stiffness tensor under the acquisition coordinate system. The relationship between this new stiffness tensor and the stiffness tensor (1) above is defined by a Bond transformation (Winterstein, 1990). The new stiffness tensor can be obtained by rotating the vertical fracture system clockwise about the vertical axis with the angle

between the fracture strike and the survey line. These form the basis from which one can start to evaluate and understand the effects of fractured-induced azimuthal anisotropy.

Apart from the elastic constants (1), there are also other sets of parameters for describing the fractured TIH medium in the literature. For example, Hudson (1981) used geometric parameters such as fracture density, aspect ratio and fracture contents; Shoenberg and Douma (1988) introduced fracture compliances for a more general representation. In the other hand, Thomsen (1986) proposed a set of parameters which are linked to practical seismic measurements. Next I will introduce the Thomsen parameters and the Hudson fracture parameters, and establish the link between them. Some basic velocity effects will also be discussed. Note that the Thomsen parameters will be used to illustrate the effects of fracture-induced azimuthal anisotropy throughout the paper.

1.1 Thomsen and Fracture Parameters

Following Thomsen (1986), for the TIH medium described by the elastic constants (1), the Thomsen parameters are defined as:

$$\varepsilon = \frac{C_{33} - C_{11}}{2C_{11}}$$

$$\delta = \frac{2C_{66} + C_{13} - C_{11}}{C_{11}} \quad (2)$$

$$\gamma = \frac{C_{44} - C_{66}}{2C_{66}}$$

Note that the original Thomsen parameters are defined for a TIV medium, and there is a 90° rotation (a bond transform, Winterstein 1990) from TIH to TIV. Also note that a simplified δ is defined here, which is the first order approximation of the original δ (Thomsen 1993, and Sayers 1995).

Assume the TIH medium is obtained by fracturing an isotropic background medium with *P*-velocity v_{p0} and *S*-velocity v_{s0}. For fracture characterization, one may wish to link the Thomsen parameters directly to the fracture parameters such as the fracture density ε_d, aspect ratio ε_{ar}, and fluid contents v_f (the compression velocity of the fluid inside the fractures). Using Hudson's (1981) model for thin fractures, the Thomsen

parameters may be expressed in terms of the fracture parameters as (Li, 1997), to the first order:

$$\varepsilon \approx 2\varepsilon_d \left(1 - \frac{v_{s0}^2}{v_{p0}^2} \right) U_{33} \qquad (3)$$

$$\delta \approx 2\varepsilon_d \left(U_{33} - \frac{v_{s0}^2}{v_{p0}^2} U_{11} \right), \quad \gamma \approx \frac{1}{2} \varepsilon_d U_{11} \qquad (4)$$

where:

$$U_{11} = \frac{16}{3} \frac{v_{p0}^2}{3v_{p0}^2 - 2v_{s0}^2} \qquad (5)$$

$$U_{33} = \begin{cases} \dfrac{4}{3} \dfrac{v_{p0}^2}{v_{p0}^2 - v_{s0}^2} & \text{if dry} \\[3mm] \dfrac{4}{3} \dfrac{v_{s0}^2}{v_f^2} \pi\varepsilon_{ar} & \text{if fluid-saturated} \end{cases} \qquad (6)$$

1.2 P-Wave Velocity Variation

One basic anisotropic effect is the *P*-wave velocity variations with incidence angle and azimuth. For the above TIH medium, assume a seismic survey line at an azimuthal angle φ to the fracture strike. Consider a *P*-wave propagating in the vertical acquisition plane. At incidence (ray) angle *i* measured from the vertical, ignoring ray deviations for weak anisotropy, the *P*-wave group velocity $v_p(i, \varphi)$ can be written as (Sena 1991):

$$v_p(i, \varphi) = v_{p0} [1 + (\delta - 2\varepsilon) \sin^2 \varphi \sin^2 i$$
$$+ (\varepsilon - \delta) \sin^4 \varphi \sin^4 i] \qquad (7)$$

where ε and δ are the Thomsen parameters, as defined in Equation (2), and v_{p0} is the background velocity. Equation (7) can also be derived from the original equations of Crampin (1981) by using the stiffness tensor under the acquisition coordinate system. Equation (7) forms the basis for normal move-out (*nmo*) velocity and interval move-out analysis.

2 PP AND PS AVO ANALYSIS: A COMPARISON

Here, I present the analytical approximations for the *PP* and *PS* AVO responses in fractured media in terms of Thomsen parameters. I also carry out a detailed numerical modelling of the *PP* and *PS* AVO responses for fractured-chalk and gas-sand reservoirs for a range of fracture parameters (fracture density ε_d, aspect ratio ε_{ar} and fluid content), with a view to improve the understanding of the sensitivity and limitations of the AVO signatures.

2.1 Analytical Approximations

Following the convention of Aki and Richards (1980), I use *i* and *j* as the average propagation angles of the upper and lower media for *P* and *S*, respectively. I assume the TIH media are obtained by fracturing isotropic background media, and use V_{P0} and V_{S0} as the average *P*- and *S*-velocities of the upper and lower background isotropic media.

In the vertical plane perpendicular to the fracture strike, the reflection coefficients r_{PP}, and r_{PS} can be written as below (Li, Kühnel and MacBeth, 1996), to the first order of the Thomsen parameters, where

$$r_{PP} = r_{PP0} + \frac{1}{2} \left[\delta_2 - \delta_1 - 2\varepsilon_2 + 2\varepsilon_1 + \frac{8V_{S0}^2}{V_{P0}^2} (\gamma_2 - \gamma_1) \right] \sin^2 i - \frac{1}{2} (\varepsilon_2 - \varepsilon_1) \sin^2 i \tan^2 i \qquad (8)$$

$$r_{PS} = r_{PS0} + \frac{\sin i}{2\cos j} \left[\frac{4V_{S0}}{V_{P0}} (\gamma_2 - \gamma_1) \cos i \cos j + (\delta_2 - \delta_1 - 2\varepsilon_2 + 2\varepsilon_1) \sin^2 i \right.$$
$$\left. - \frac{4V_{S0}^2}{V_{P0}^2} (\gamma_2 - \gamma_1) \sin^2 i + 2(\varepsilon_2 - \varepsilon_1 - \delta_2 + \delta_1) \sin^4 i \right] + \frac{1}{2} \left(\frac{\sin i}{\cos j} - \frac{\sin j}{\cos i} \right) \Delta\zeta_P \qquad (9)$$

$$\Delta\zeta_P = \frac{V_{P0}^2}{V_{P0}^2 - V_{S0}^2} \left[(\delta_2 - \delta_1 - 2\varepsilon_2 + 2\varepsilon_1) - 2(\delta_2 - \delta_1 - \varepsilon_2 + \varepsilon_1) \sin^2 i \right] \cos^2 i \qquad (10)$$

ε_k, δ_k and γ_k ($k = 1,2$) are the Thomsen parameters for the upper ($k = 1$), and lower ($k = 2$) medium, respectively; r_{PP0} and r_{PS0} are the reflection coefficients in the vertical plane parallel to the fracture strike, and are the same as the isotropic reflectivities of the background media.

To examine the effects of anisotropy, I consider the AVO gradient ($\sin^2 i$) and the near-offset ($\cos i \cos j$) terms only. (Note that when referred to various terms for r_{PS}, the common factor $\sin i / \cos j$ outside the bracket are excluded for simplicity). Substituting Equation (10) into Equation (9) and ignoring the higher order term of $\sin^2 i$ gives (11) and (12).

Equations (1) and (2) are only valid in the vertical symmetry plane perpendicular to the fracture and are independent of azimuth. Despite this, the differential reflectivity between the planes perpendicular and parallel to the fracture strike ($r_{PP} - r_{PP0}$, and $r_{PS} - r_{PS0}$) may give some indications of the magnitudes of the azimuthal variations.

Some immediate observations can be drawn from the first two equations. Firstly, the effects of anisotropy on the AVO response of both *PP* and *PS* waves are of first order and cannot be ignored. Secondly, the anisotropy affects the *PS* waves more than the *PP* wave, through the near-offset term $\cos i \cos j$, indicating that the *PS* AVO response and its differential variations ($r_{PS} - r_{PS0}$) are more sensitive to anisotropy, or fracturing, than the *PP* AVO response and its differential variations ($r_{PP} - r_{PP0}$). Thirdly, a smaller

angular coverage may be required to reveal the effects of the *PS* AVO response because of the presence of the near-offset term ($\cos i \cos j$).

2.2 Numerical Modelling

I consider two typical models from the North sea: one is a chalk-fractured reservoir model (Fig. 1), and the other is a traditional shale over gas sand model (Fig. 2). Chalk reservoirs usually have low/high impedance contrast for the top interface. Whereas the bottom interface may have either a low/high, or high/low impedance contrast. In this case, I compare the AVO responses for both the top and the bottom interfaces. For shale over gas sand, I only compare the responses for the top interface.

ρ = 2.35 g/cm	V_p = 2563 m/s V_s = 994 m/s	CLAYSTONE
ρ = 2.08 g/cm	V_p = 2903 m/s V_s = 983 m/s	CHALK A
ρ = 2.2 g/cm	V_p = 3174 m/s V_s = 1326 m/s	CHALK B

Figure 1

A fractured-chalk model from the North Sea.

$$r_{PP} = r_{PP0} + \frac{1}{2}\left[\delta_2 - \delta_1 - 2\varepsilon_2 + 2\varepsilon_1 + \frac{8V_{S0}^2}{V_{P0}^2}(\gamma_2 - \gamma_1)\right]\sin^2 i \tag{11}$$

$$r_{PS} = r_{PS0} + \frac{\sin i}{2\cos j}\left[\frac{V_{P0}^2}{V_{P0}^2 - V_{S0}^2}(\delta_2 - \delta_1 - 2\varepsilon_2 + 2\varepsilon_1) + \frac{4V_{S0}^2}{V_{P0}^2}(\gamma_2 - \gamma_1)\cos i \cos j\right.$$

$$-\frac{V_{P0}V_{S0}}{V_{P0}^2 - V_{S0}^2}(\delta_2 - \delta_1 - 2\varepsilon_2 + 2\varepsilon_1)\cos i \cos j - \frac{4V_{S0}^2}{V_{P0}^2}(\gamma_2 - \gamma_1)\sin^2 i \tag{12}$$

$$+(\delta_2 - \delta_1 - 2\varepsilon_2 + 2\varepsilon_1)\sin^2 i - \frac{V_{P0}^2}{V_{P0}^2 - V_{S0}^2}(3\delta_2 - 3\delta_1 - 4\varepsilon_2 + 4\varepsilon_1)\sin^2 i\right]$$

ρ = 2.3 g/cm	V_p = 3048 m/s	
	V_s = 1574 m/s	SHALE
ρ = 2.19 g/cm	V_p = 2183 m/s	GAS SAND
	V_s = 1502 m/s	

Figure 2

A typical fractured gas-sand model.

During the numerical calculations, the maximum incidence angle is set to 50°. The modelling reveals:

1) For the models studied here, the *PP* AVO response appears to be elliptical for the top interface, but non-elliptical for the bottom interface (Fig. 3). This is also true for the *PS* AVO response (Fig. 3).

2) Changing of aspect ratio and fracture density has more influence on the *P*-AVO response from the bottom interface than that from the top (Fig. 3). However, the opposite is true for the *PS* wave.

3) Overall, the *PS* AVO response is more sensitive to fracturing, than the *PP* AVO response (Figures 3 and 4), both in terms of azimuthal variation and offset variation (Fig. 4). In particular, the *PS* AVO

response shows significant variations in the near offset, while variations in the *PP* AVO response can only be identified in the far offset (Fig. 4).

These modelling results, particularly item 3 above, broadly agree with the observations from the analytical approximations in the previous section (e.g. the second observation).

3 AZIMUTHAL P-WAVE ANALYSIS: A REVIEW

Here, I examine the azimuthal variation of *P*-wave amplitude, velocity and move-out in fractured media. All these effects are expressed in analytical form under the assumption of weak anisotropy, which enables some understanding of various dependencies, and allows the development of processing algorithms to extract these effects from multicomponent seismic data.

3.1 P-Wave Amplitude

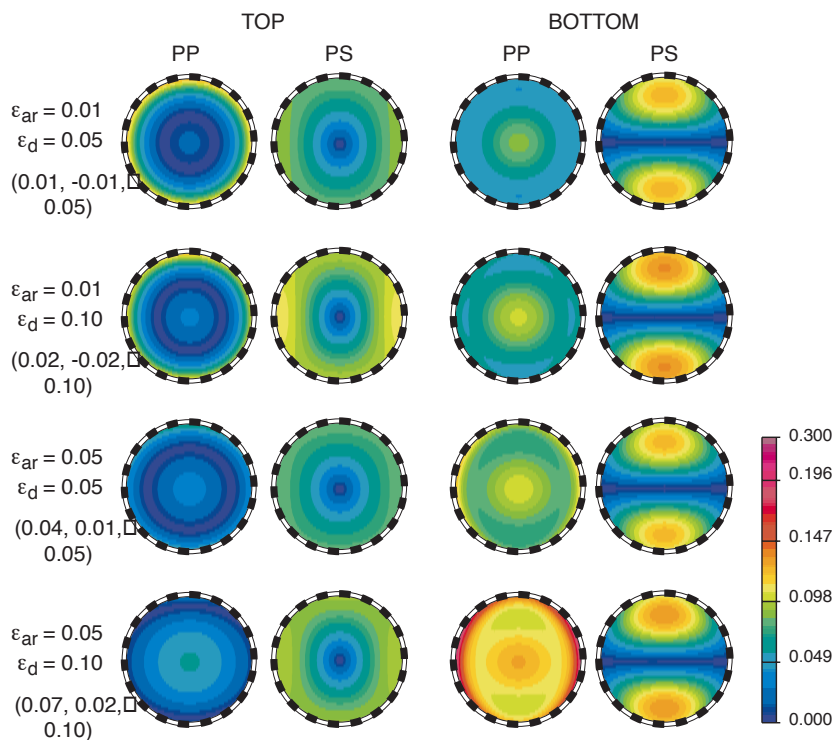When the survey line is at an oblique angle from the fracture strike, the vertical acquisition plane is a

Figure 3

Comparison of *PP* and *PS* reflection coeffients for the chalk model in Figure 1 with oil-filled fractures. ε_{ar} is the aspect ratio, and ε_d is the fractured density. The numbers in the bracket such as (0.01, –0.01, 0.05) represent the Thomsen parameters (ε, δ, γ), respectively.
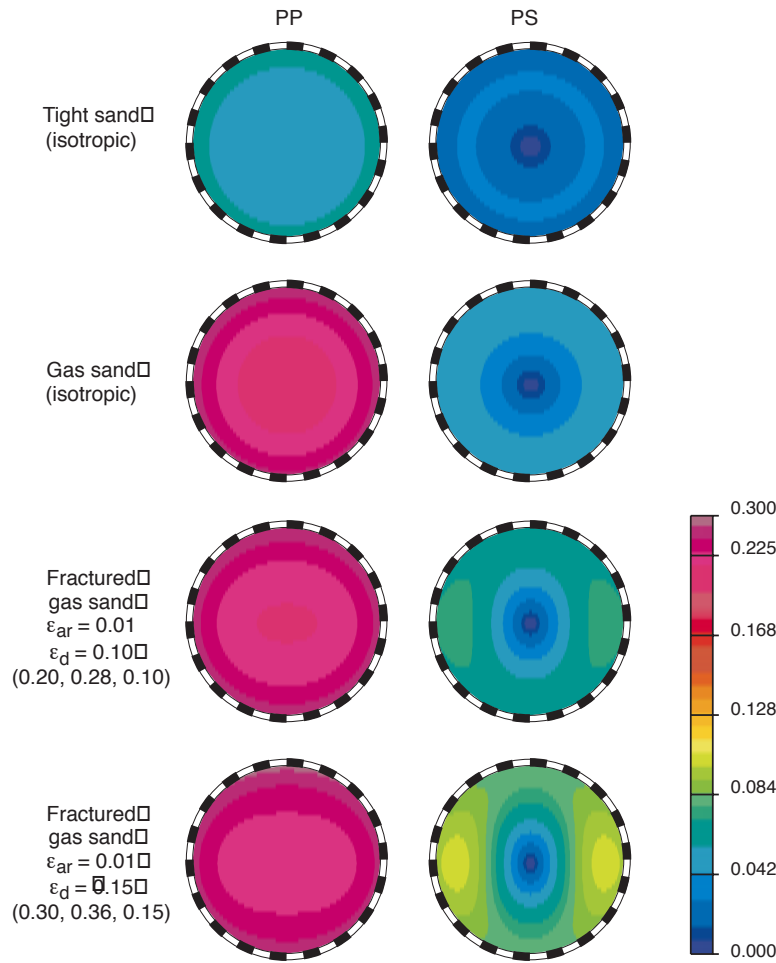
Figure 4

Comparison of *PP* and *PS* reflection coeffients for the gas-sand in Figure 2. ε_{ar} is the aspect ratio, and ε_d is the fractured density. The numbers in the bracket such as (0.20, 0.28, 0.10) represent the Thomsen parameters (ε, δ, γ), respectively.

non-symmetry plane. Wave propagation in this plane is coupled and strictly speaking, analytical and explicit equations to describe amplitude variations accurately in this plane do not exist, particularly for mode conversion and for shear-waves. Despite this, for weak anisotropy, ignoring ray deviation, approximate equations can still be derived, particularly for *PP* waves. One of the ways to derive these equations is to use the elastic tensor under the acquisition coordinate system.

Various forms of approximations for azimuthal variations of *PP* reflections have been reported (Rüger, 1996; Li and Mavko, 1996). However for regions of interests (incidence angle beyond 15°), as shown by the authors, accuracy of these approximations is greatly reduced. One particularly useful aspect predicted by these approximations is the azimuthal variation of *PP* reflection for fixed offset.

For a fixed offset with sufficiently large offsets, the reflection amplitude as a function of source-receiver azimuth (φ), as measured from the fracture strike, has the following form approximately:

$$R_{pp}(\varphi) = A + B \cos^2\varphi \qquad (13)$$

where *A* and *B* are constants.

Mallick *et al.* (1996) first presented Equation (13) as an empirical expression from numerical modelling, and applied it to 3D land data to quantify the fracture strike. Following Mallick *et al.* (1996), Lynn *et al.* and MacBeth *et al.* (1997) also applied this to real data. Equation (13) forms the basis for azimuthal *P*-AVO analysis.

3.2 P-wave Normal Move-out Velocity

Assume the TIH medium, as defined by Equations (1) and (2), containing a single horizontal reflector. The

short spread normal move-out (*nmo*) velocity v_{nmo} for a given ray at azimuth φ measured from the fracture strike can be written as (Sena 1991):

$$v_{nmo}^2(\varphi) = v_{p0}^2 \left[1 + 2(\delta - 2\varepsilon) \sin^2 \varphi \right]$$
$$= C + D \sin^2 \varphi \qquad (14)$$

This leads to:

$$v_{nmo}^2(\varphi) = v_{nmo}^2(0) \cos^2 \varphi + v_{nmo}^2(90°) \sin^2 \varphi \qquad (15)$$

where $v_{nmo}(0)$ is the *nmo* velocity at azimuth parallel to the fracture strike and $v_{nmo}(90°)$ is the *nmo* velocity at azimuth perpendicular to the fracture strike.

Equation (14) has a similar form as the *P*-wave azimuthal AVO Equation (13), and Equation (15) reveals a simple elliptical variation of the *nmo* velocity along the azimuthal direction. Thus, it is possible to recover the fracture strike from the move-out velocities measured from the different survey lines with difference azimuths, as shown in Sena (1991) using synthetic data, and in Corrigan *et al.* (1996) using a real data example. Depending on known numbers of parameters, it usually requires three azimuthal measurements to recover the fracture strike.

Grechka and Tsvankin (1996) generalized Equation (15) for generally inhomogeneous anisotropic media. They showed that this simple elliptical variation of short spread *nmo* velocity is valid for generally inhomogeneous anisotropic media, although Equation (15) is derived using the weak anisotropy assumption.

3.3 P-wave Interval Move-out

Assume a fractured layer with azimuthal anisotropy overlain by a weakly anisotropic overburden (Fig. 5). Consider two orthogonal line-azimuths at angles ϕ and $\phi - \pi/2$ to the fracture strike, respectively (lines 1 and 2, Fig. 6). The azimuthal difference of the interval move-out for the fractured layer between these two lines also shows a cos 2ϕ variation (Li, 1997):

$$\Delta t(\phi, x) = E(x, \varepsilon, \delta) \cos 2\phi \qquad (16)$$

where E is a function related to the acquisition geometry and the fractured layer.

Consider another pair of orthogonal lines separated by an angle φ_0 from the first pair (lines 3 and 4, Fig. 6), yielding:

$$\tan 2\phi = \frac{(\Delta t_2 - \cos 2\varphi_0 \, \Delta t_1)/\sin 2\varphi_0}{\Delta t_1} \qquad (17)$$
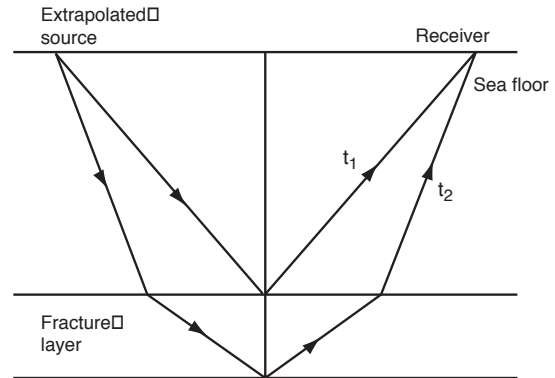

Figure 5

The ray-paths of *PP* reflections from the top and bottom of a fractured layer. Note that an extrapolated source is assumed on the sea floor.
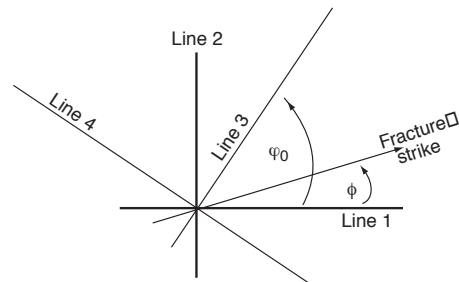

Figure 6

Four-line configuration for fracture detection.

where $\Delta t_1 = \Delta t(\phi, x)$, and $\Delta t_2 = \Delta t(\phi + \varphi_0, x)$. Denote the numerator in Equation (17) as $\Delta t_2'$. Thus, for the four line configuration in Figure 6, the cross plot of Δt_1 versus $\Delta t_2'$ shows a linear trend, indicating the direction of 2ϕ. A least square analysis of the cross-plot can be used to estimate the fracture strike as:

$$\phi = \frac{1}{4} \tan^{-1} \left\{ \frac{2 \sum_x \Delta t_1 \Delta t_2'}{\sum_x \Delta t_1^2 - \Delta t_2'^2} \right\} \qquad (18)$$

Li (1998) applied this method to real data.

4 PS POLARIZATION ANALYSIS

P-wave anisotropic effects occur only with wide azimuthal coverage. Consequently, the effects are subtle and often difficult to recover from the data. In contrast,

shear-wave anisotropic effects occur at near vertical propagation and are relatively stable and robust.

When a shear-wave enters a fracture-induced anisotropic medium, it splits into two modes which travel with different speeds. For near vertical propagation, the fast shear-wave polarises parallel to the fracture strike, and the slow wave polarises perpendicular to the strike. Furthermore the normalised time-delay between the fast and slow split shear-wave:

$$\varepsilon_{td} = \frac{t_2 - t_1}{t_1} = \frac{C_{44} - C_{66}}{2C_{66}} - \frac{1}{2}\,\varepsilon_{td}^2 \approx \gamma \qquad (19)$$

is a measure of the Thomsen parameter γ which is in turn related to the fracture density (porosity) in the medium. Thus *PS* wave polarization analysis provides an effective way to determine the fracture strike and density.

Next, I will present three processing methods for recovering the polarization azimuth and time delay from *PS* waves for different sea-floor acquisition geometries. The first one is for a 2D geometry where the source boat sails along the receiver cable. In this case, an optimum method based on rotation and correlation analysis is proposed. The second and the third method is for a 3D geometry where the source boat sails across (perpendicular to) the receiver cable. In this case, deterministic methods based on azimuthal analysis of *PS* waves are proposed. (Note that the proposing use of deterministic methods does not necessarily mean that the optimum method is less robust or less accurate. Depending on data quality, the objective function used by the optimum method may have local maxima which lead to non-unique solutions).

4.1 Rotation Analysis for 2D Acquisition

Consider a 2D acquisition over horizontally stratified media with uniform azimuthal anisotropy. Further assume a *PS* raypath with the conversion point at the reflector, and a displacement vector confined to the horizontal plane, ϕ representing the polarization azimuth of the fast shear wave (Fig. 7). The recorded radial and transverse components can be written as:

$$\begin{pmatrix} V_r(t) \\ V_t(t) \end{pmatrix} = \begin{pmatrix} \cos\phi & -\sin\phi \\ \sin\phi & \cos\phi \end{pmatrix} \begin{pmatrix} S_1(t) \\ S_2(t) \end{pmatrix}$$
$$= \mathbf{R}(\phi) \begin{pmatrix} S_1(t) \\ S_2(t) \end{pmatrix} \qquad (20)$$

where $\mathbf{R}(\phi)$ is the 2D rotation matrix, and $S_1(t)$ and $S_2(t)$ represent the amplitudes of the fast and slow waves, respectively.
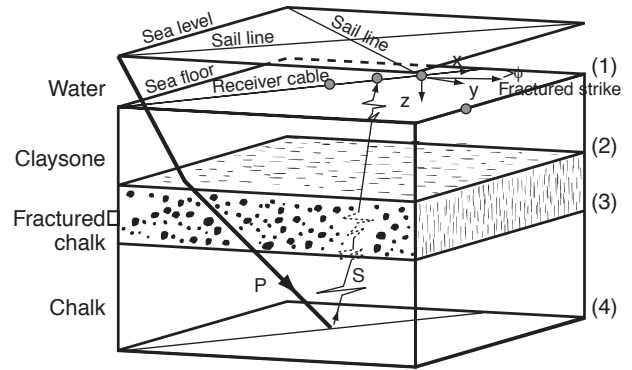

Figure 7

A four-layer model showing converted shear-waves in 3C sea-floor seismic acquisition over fractured media. A conversion at the reflection point is assumed. Numbers (1), (2), (3) and (4) are the interface numbers.

Assuming that the fast and slow shear-wave have similar waveforms with only a time delay Δt, $S_1(t) = S(t)$, $S_2(t) = S(t - \Delta t)$, Equation (20) can be solved by rotation analysis based on an objective function which measures the similarity of the two waveforms. Rotating the radial and transverse components with an angle α gives the rotated components $R_{vr}(\alpha, t)$ and $R_{vt}(\alpha, t)$ as:

$$\begin{pmatrix} R_{vr}(\alpha, t) \\ R_{vt}(\alpha, t) \end{pmatrix} = \mathbf{R}^T(\alpha) \begin{pmatrix} V_r(t) \\ V_t(t) \end{pmatrix} \qquad (21)$$

An objective function $F(\alpha, \tau)$ may be defined as:

$$F(\alpha, \tau) = \sum_t R_{vr}(\alpha, t)\, R_{vt}(\alpha, t + \tau) \qquad (22)$$

Thus, the optimization process is to search for a rotation angle $\alpha = \phi$ and time shift $\tau = \Delta t$, which maximizes $F(\alpha, \tau)$ (Fig. 8). MacBeth and Crampin (1991) gave a good review of this kind of techniques. Donati and Brown (1995) also used similar techniques for processing converted shear-waves in land acquisitions. Note that if there is more than one anisotropic layer, one may proceed in a layer-stripping fashion.
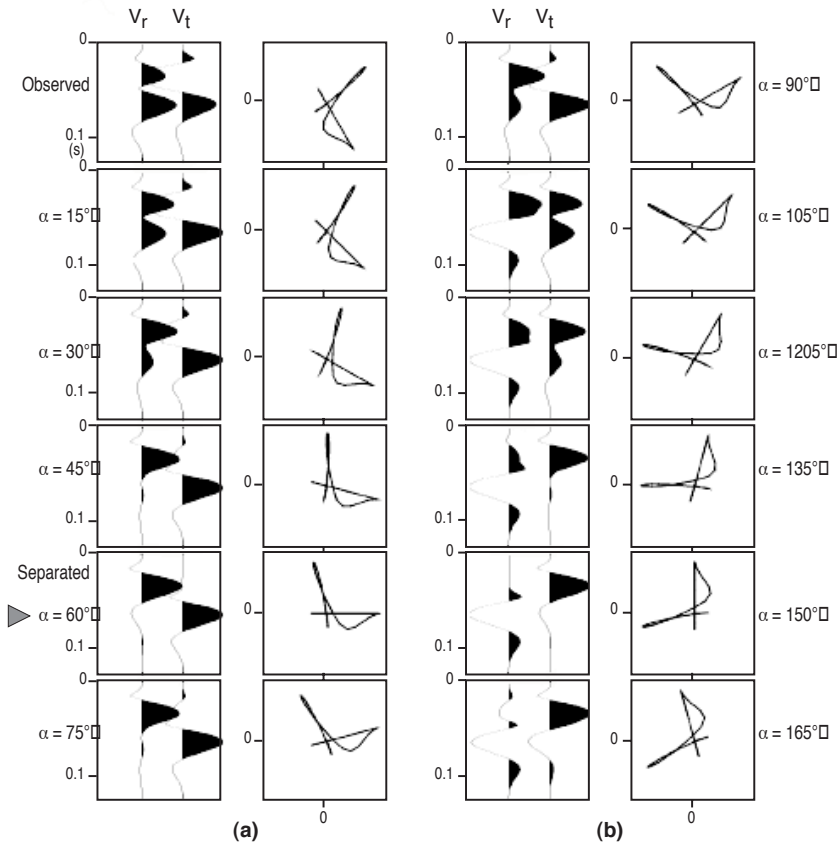
Figure 8

Determining the polarization azimuth based on the similarity of the fast and slow waves.

(a) From top to bottom, rotation angles between 0 and 75°. (b) The corresponding angles between 90° and 165°. The increment is set to 15°.

Note that the two waveforms are most similar at rotation angle $\alpha = 60°$, indicating the polarization of the fast shear-wave.

4.2 Azimuthal Analysis for 3D Acquisition

Consider the off-line shooting cross-geometry as shown in Figure 9 over horizontally stratified media with uniform azimuthal anisotropy. For the source-receiver azimuth φ, the horizontal components V_r and V_t in the local coordinate system (r, t) can be written as, for shear-waves only:

$$\begin{pmatrix} V_r(t_0, \Delta) \\ V_t(t_0, \Delta) \end{pmatrix} = \mathbf{R}^T(\Delta) \begin{pmatrix} \lambda_1(t_0) & 0 \\ 0 & \lambda_2(t_0) \end{pmatrix} \times \mathbf{R}(\Delta) \begin{pmatrix} PS(t_0) \\ 0 \end{pmatrix} \tag{23}$$

where t_0 is time after *PS* conversion, $\Delta = \phi - \varphi$ is the angle between the fracture strike and the source-receiver azimuth, $\mathbf{R}$ is a 2D rotation matrix, λ_1 and λ_2 are propagating functions for the fast and slow wave, respectively, and $PS(t)$ is the effective shear-wave source due to conversion.

Note that based on Huygens' principle, the wavefront upon conversion can be treated as an effective source which excites the subsequent up-going converted shear-wave wave. The magnitude of this effective shear-wave source is related the raypath of the first *P*-wave leg and the *P*-to-*S* conversion coefficient at the interface. Also note that during acquisition the horizontal geophones are actually orientated in the inline and crossline directions of the acquisition coordinate system (x, y). Assuming true vector fidelity for the geophones, the radial and transverse components v_r and v_t under the local coordinate system (r, t) are related to the recorded components v_x and v_y as:

$$\begin{pmatrix} V_r(t_0, \Delta) \\ V_t(t_0, \Delta) \end{pmatrix} = \mathbf{R}(\varphi) \begin{pmatrix} V_x(t_0) \\ V_y(t_0) \end{pmatrix} \tag{24}$$

It follows from Equation (23) that:

$$\begin{aligned} V_t(t_0, \Delta) &= 0 \ \text{ for } \Delta = 0, \text{ or } \pi/2 \\ V_t(t_0, -\Delta) &= -V_t(t_0, \Delta) \end{aligned} \tag{25}$$

This implies that if the source-receiver azimuth is parallel or perpendicular to the fracture strike, the energy in the transverse component vanishes, and that the wave forms show a polarity change.
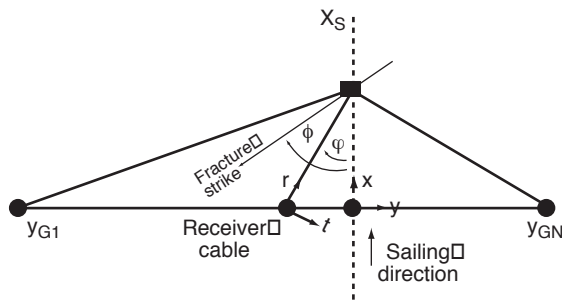
Figure 9

A plan view of a 3D cross geometry. (x, y) is the acquisition coordinate system; (r, t) is the local system associated with source-receiver azimuth φ; ϕ is the fracture strike measured from the sailling direction x. y_{G1} and y_{GN} are the offsets for the first and the *Nth* (last) geophone, and x_S is the source offset. Note that an asymmetric geometry is used for maximising the azimuthal coverage.

Thus, a two-stage procedure can be used for anisotropy analysis. The first stage is to use the azimuthal gathers from the crossline-shooting to estimate the polarization azimuth, based on the two criteria: polarity reversal and minimum amplitude. The second stage is to use the inline-shooting gathers to estimate the time delay of the split shear-waves. Note that Garotta and Granger (1988) used the minimum amplitude criterion. However, the polarity reversal criterion could be more robust for sea-floor data with high signal to noise (S/N) ratio.

Full-wave modelling by the reflectivity method (Taylor 1990) for the model in Figure 7 and Table 1 is used to verify the azimuthal analysis procedures. In the model, the fracture strike is set to $\phi = 30°$, measured from the boat direction clockwisely (Fig. 9). One crossline shooting gather (source offset $x_S = 1$ km, Fig. 10) and one inline-shooting gather ($x_S = 0$, Fig. 11) are generated. Details of the analysis sequence are:

– sorting the data into azimuthal gathers (Figs. 10a and 10b) and covering as many azimuthal directions as possible (Figs. 10a and 10b);
– rotating the horizontal components by φ into the local coordinate system (r, t) (Figs. 10c and 10d);
– determining the polarization azimuth ϕ by applying the polarity reversal and minimum amplitude criteria (Fig. 10d);
– rotating the inline-shooting gathers by angle ϕ to separate the fast and slow shear-wave and to determine the time delays (Fig. 11).

TABLE 1

Layer parameters used in the study

Layers	ρ (g/cm³)	v_p (m/s)	v_s (m/s)	Thickness (m)
Water	1.00	1500	–	100
Claystone	1.97	1990	1000	1200
Frac. chalk*	2.2	3500	1750	300
Chalk	2.1	3080	1540	700
Clastic	2.37	4200	2100	–

* fractured chalk with $\varepsilon_d = 0.10$ and $\varepsilon_{ar} = 0.01$.
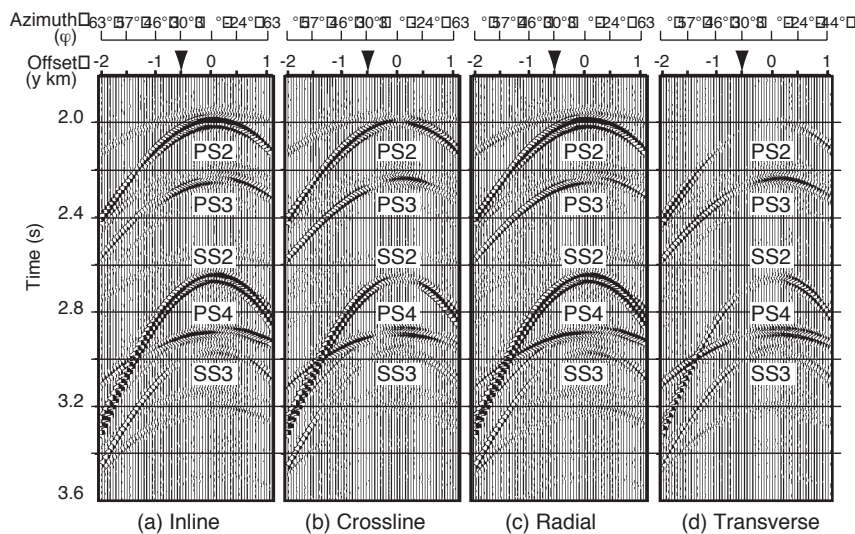

Figure 10

Azimuthal gathers of (a) inline, (b) crossline, (c) radial and (d) transverse components, calculated from the model in Figure 7 and Table 1 for source offset $x_S = 1$ km, $y_{G1} = -2$ km and $y_{GN} = 1$ km with 50 m spacing. The arrow marks the critical azimuth with the polarity reversal and amplitude minimum. Label PS_2 stands for the *PS* conversion from interface 2, and PS_3 for the conversion from interface 3, etc.
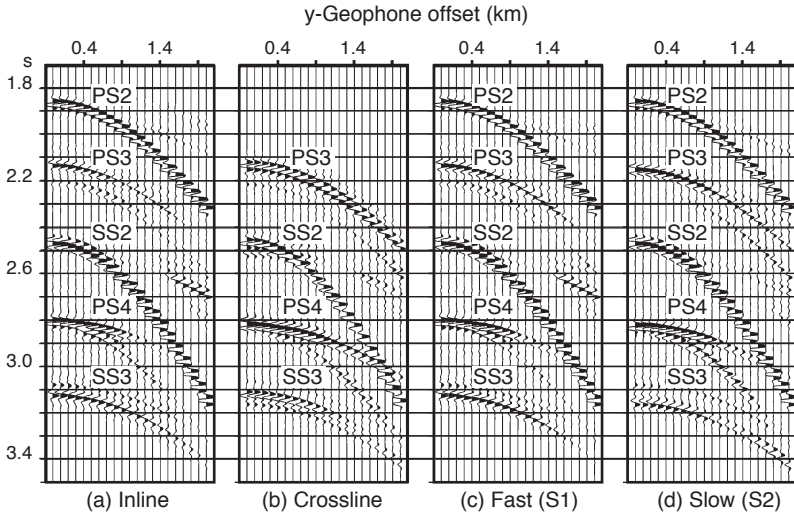
Figure 11

Inline-shooting gathers of (a) inline, (b) crossline, (c) *S*1 (fast *S*-wave) and (d) *S*2 (slow *S*-wave) components for source offset $x_S = 0$, $y_{G1} = -2$ km and $y_{GN} = 1$ km with 50 m spacing. The shear-waves in (c) and (d) are clearly separated with similar forms and better continuity than those in (a) and (b). Note *SS*2 indicating the *S*-wave reflection from interface 2, and the conversion taking place at the seabed.

The polarization azimuth is determined at 30°using the above method for Figure 10d. The fast and slow shear-waves are clearly separated in Figures 11c and 11d after rotating the inline gathers in Figures 11a and 11b by 30°. Approx 20 ms of time delay can be identified for the converted waves beneath the fractured chalk (*PS*3, *PS*4, *SS*3, Figures 11c and 11d), indicating about 10% anisotropy.

4.3 Rotation Analysis for 3D Acquisition

Consider any orthogonal pairs of source-receiver azimuths 1 and 2 in the 3D cross geometry, as shown in Figure 12. Azimuth 1 is at angle φ from the boat direction, and azimuth 2 at angle $\pi/2 - \varphi$ to the boat direction (Fig. 12). For these two azimuths, after correcting the ray-path difference by move-out correction, the recording components V_{1x} and V_{1y} for azimuth 1 can be written as:

$$\begin{pmatrix} V_{1x}(t_0) \\ V_{1y}(t_0) \end{pmatrix} = \mathbf{R}^T(\phi) \begin{pmatrix} \lambda_1(t_0) & 0 \\ 0 & \lambda_2(t_0) \end{pmatrix} \mathbf{R}(\phi - \varphi) \begin{pmatrix} PS_1(t_0) \\ 0 \end{pmatrix}$$

(26)

and V_{2x} and V_{2y} for azimuth 2 as:

$$\begin{pmatrix} V_{2x}(t_0) \\ V_{2y}(t_0) \end{pmatrix} = \mathbf{R}^T(\phi) \begin{pmatrix} \lambda_1(t_0) & 0 \\ 0 & \lambda_2(t_0) \end{pmatrix} \mathbf{R}(\phi - \varphi) \begin{pmatrix} 0 \\ PS_2(t_0) \end{pmatrix}$$

(27)

where t_0 is the move-out-corrected two-way time, λ_1 and λ_2 are propagating functions for the fast and slow wave, respectively, and $PS_1(t)$ and $PS_2(t)$ are the effective shear-wave sources at azimuths 1 and 2, respectively.
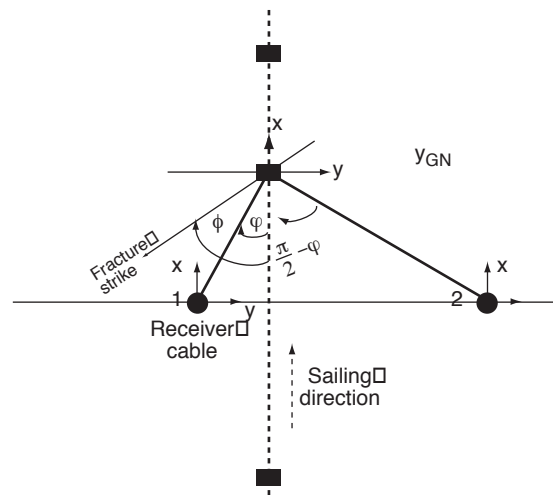

Figure 12

Same as Figure 9, but an orthogonal pair of source-receiver azimuths is selected for analysis.

Thus the recording components for the two azimuths, Equations (26) and (27), can be combined as:

$$\begin{pmatrix} V_{1x}(t_0) & V_{2x}(t_0) \\ V_{1y}(t_0) & V_{2y}(t_0) \end{pmatrix} = \mathbf{R}^T(\phi) \begin{pmatrix} \lambda_1(t_0) & 0 \\ 0 & \lambda_2(t_0) \end{pmatrix}$$
$$\times \mathbf{R}(\phi - \varphi) \begin{pmatrix} PS_1(t_0) & 0 \\ 0 & PS_2(t_0) \end{pmatrix}$$

(28)

Note that the amplitudes of the propagating functions are usually not equal to each other, nor the effective shear-wave sources. However, Equation (28) can still be simplified by compensating for the difference in the effective sources, so that the right-most matrix representing the effective shear-wave sources in Equation (28) may be reduced to the product of a scalar

with the unit matrix. Rotating the two horizontal components by angle φ, the ratio of the effective sources $PS_1(t_0)/PS_2(t_0)$ can be estimated from the off-diagonal elements of the rotated data matrix. This ratio can then be used as a scaling factor to compensate for the difference between the effective sources. The rotated and amplitude-corrected data matrix $\mathbf{D}_c(t_0)$ can be written as:

$$\mathbf{D}_c(t_0) = \mathbf{R}^T(\phi - \varphi) \begin{pmatrix} S_1(t_0) & 0 \\ 0 & S_2(t_0) \end{pmatrix} \mathbf{R}(\phi - \varphi) \quad (29)$$

Thus, the polarization azimuth ϕ can be solved by minimizing the off-diagonal elements of $\mathbf{D}_c(t_0)$.

A similar method to the above has been successfully used for processing converted waves in 3D land acquisitions by Gaiser (1997). Here, I have reformulated the method for sea-floor recordings, and my main purpose is for comparison with the previous azimuthal analysis method. Compared with the previous one, this method is subjected to two more additional pre-processing steps: the proper correction of the *nmo* move-out and the proper scaling of the off-diagonal components to compensate for the differences in the conversion coefficients because the raypath differences. Thus this procedure may be best suited for post-stack analysis, as in the land case. This means that a full 3D coverage with a 2D array of three-component geophones on the sea-floor is needed.

Post-stack analysis may be necessary if the signal to noise ratio of the pre-stack data is relatively low. To prepare for the post-stack analysis, the full dataset may be binned into orthogonal narrow-azimuthal data volumes. These azimuthal data volumes may then be processed separately to obtain orthogonal azimuthal stacks. Equation (29) may then be applied to these orthogonal azimuthal stacks.

5 DISCUSSION AND CONCLUSIONS

I have examined some of the fundamental aspects for both *PP* and *PS* waves propagating in fracture-induced transverse anisotropic media with a horizontal symmetry axis (TIH), and have presented various methods to recover the fracture strike and density from the recorded *PP* and *PS* waves in sea-floor acquisitions. *P*-wave effects occur only with wide azimuth and have proved to be effective in determining fracture strike. In contrast, *PS* wave effects occurs at near vertical

propagations and have proved to be effective in determining both the fracture strike and density. Reliable methods for recovering aspect ratio and fracture content are yet to be developed.

To conclude, for *P*-wave analysis in the presence of azimuthal anisotropy, the azimuthal variations in *PP* amplitude, normal move-out velocity, and interval move-out show elliptical shapes, which can be used to determine the fracture strike of the fractured media. The use of azimuthal interval move-out for detecting fracture strike shows some distinct features. Compared with the velocity approach, evaluation of the interval move-out provides more quality control and easy means for overburden correction. A configuration of four intersecting survey lines, forming two pairs of orthogonal source-receiver azimuths, can be used for determining the fracture strike. The method may be particularly useful in marine exploration with repeated surveys of various vintages where continuous azimuthal coverage is often not available.

For *PS* wave polarization analysis, a polarity reversal and amplitude dimming will occur in the azimuthal gathers of the transverse component. This feature provides robust and accurate estimates of the fracture strike using a 3D cross geometry where the source boat sails across the receiver cable. After separating the fast and slow waves the time delay can be estimated from the inline shooting gathers. Alternatively, one can also use rotation analysis for determining the fracture strike for the 3D cross geometry. In this case, horizontal components within orthogonal pairs of source-receiver azimuths may be sorted into 2 x 2 data matrices after correcting for moveout and amplitude differences. The polarization azimuth can then be determined by minimizing the off-diagonal elements of these data matrices.

ACKNOWLEDGMENT

REFERENCES

Aki K. and Richards P.G. (1980) *Quantitative Seismology, Theory and Methods,* W.H. Freeman and Co.

Corrigan D., Withers R., Darnall J. and Skopinski T. (1996) Fracture mapping from azimuthal velocity analysis using 3D surface seismic data. *66th Internat. Mtg., Soc. Explor. Geophys.,* Expanded Abstracts, 1834-1837.

Crampin S. (1981) A review of wave motion in anisotropic and cracked elastic media. *Wave Motion,* 3, 343-391.

Crampin S. and Lovell J.H. (1991) A decade of shear-wave splitting in the Earth's crust: what does it mean? What use can we make of it? and what should we do next? *Geophys. J. Internat.,* 107, 387-407.

Donati M. and Brown R.J. (1995) Birefringence study on 3-C/2-D: Barinas Basin (Venezuela). *65th Internat. Mtg., Soc. Explor. Geophys.,* Expanded Abstracts, 723-726.

Gaiser J.E. (1997) 3-D converted shear wave rotation with layer stripping. *U.S. Patent* no. 5,610,875.

Grechka V. and Tsvankin I. (1996) 3-D description of normal move-out in anisotropic media. *66th Internat. Mtg., Soc. Explor. Geophys.,* Expanded Abstracts, 1487-1490.

Hudson J.A. (1981) Wave speeds and attenuation of elastic waves in material containing cracks. *Geophys. J. Roy. Astr. Soc.,* 64, 133-150.

Garotta R. and Granger P.Y. (1988) Acquisition and processing of 3C × 3-D data using converted waves. *58th Internat. Mtg., Soc. Explor. Geophys.,* Expanded Abstracts, 995-997.

Lefeuvre F. (1994) Fracture related anisotropy detection and analysis: "and if the *P*-waves were enough?". *64th Internat. Mtg., Soc. Explor. Geophys.,* Expanded Abstracts, 942-945.

Li T. and Mavko G. (1996) Fracture signatures on *P*-wave AVOZ. *66th Internat. Mtg., Soc. Explor. Geophys.,* Expanded Abstracts, 1818-1821.

Li X.Y. (1997) Viability of azimuthal variation in P-wave move-out for fracture detection. *67th Internat. Mtg. Soc. Explor. Geophys.,* Expanded Abstracts, 1555-1558.

Li X.Y. (1998) Azimuthal move-out analysis for fracture detection in marine streamer data. *60th EAGE Meeting,* Expanded Abstracts, P-154.

Li X.Y. and Crampin S. (1993) Approximations to shear-wave velocity and move-out equations in anisotropic media. *Geophys. Prosp.,* 41, 833-857.

Li X.Y., Kühnel T. and MacBeth C. (1996) Mixed mode AVO response in fractured media. *66th Internat. Mtg., Soc. Explor. Geophys.,* Expanded Abstracts, 1822-1825.

Lynn H.B. Simon K.M. Bates C.R. and Van Dok R. (1996) Naturally fractured gas reservoir's seismic characterization. *66th Internat. Mtg., Soc. Explor. Geophys.,* Expanded Abstracts, 1360-1363.

MacBeth C. and Crampin S. (1991) Comparison of signal processing techniques for estimating the effects of anisotropy. Geophys. Prosp., 39 357-385.

MacBeth C. Jakubowicz H. Kirk W. Li X.Y. and Ohlsen F. (1997) Fracture-related variations with offset and azimuth in marine seismic data. *67th Internat. Mtg., Soc. Explor. Geophys.,* Expanded Abstracts, 195-198.

Mallick S. Craft K.L. Meister L.J. and Chambers R.E. (1996) Computation of principal directions of azimuthal anisotropy from *P*-wave seismic data. *66th Internat. Mtg., Soc. Explor. Geophys.,* Expanded Abstracts, 1862-1865.

Rüger A. (1996) Variation of *P*-wave reflectivity with offset and azimuth in anisotropic media. *66th Internat. Mtg., Soc. Explor. Geophys.,* Expanded Abstracts, 1810-1813.

Sayers C.M. (1995) Simplified anisotropy parameters for transversely isotropic sedimentary rocks: *Geophysics,* 60, 1933-1935.

Sena A.G. (1991) Seismic travel time equations for azimuthally anisotropic and isotropic media: Estimation of interval elastic properties. *Geophysics,* 56, 2090-2101.

Schoenberg M. and Douma J. (1988) Elastic wave propagation in media with parallel fractures and aligned cracks. *Geophys. Prosp.,* 36, 571-590.

Taylor D.B. (1990) *Aniseis Manual, Applied Geophysical Software.*

Thomsen L.A. (1986) Weak elastic anisotropy. *Geophysics,* 51, 1954-1966.

Thomsen L.A. (1988) Reflection seismology over azimuthally anisotropic media. *Geophysics,* 53, 304-313.

Thomsen L.A. (1993) Weak anisotropic reflections. In: *Offset-dependent reflectivity; theory and practice of AVO analysis* (Eds. J.P. Castagna and M.M. Backus), SEG Special Publication, 103-111.

Tsvankin I. (1995) Inversion of move-out velocities for horizontal transverse isotropy. *65th Internat. Mtg., Soc. Explor. Geophys.,* Expanded Abstracts, 735-738.

Tsvankin I. (1996) *P*-wave signatures and notation for transversely isotropic media: An overview. *Geophysics,* 61, 467-483.

Tsvankin I. (1996) Effective parameters and *P*-wave velocity for azimuthally anisotropic media. *66th Internat. Mtg., Soc. Explor. Geophys.,* Expanded Abstracts, 1850-1853.

Winterstein D.F. (1990) Velocity anisotropy terminology for geophysicists. *Geophysics,* 55, 1070-1088.